

Characterization of ground penetrating radar signal during simulated corrosion of concrete reinforcement

Tesic, Ksenija; Baricevic, Ana; Serdar, Marijana; Gucunski, Nenad

Source / Izvornik: **Automation in construction, 2022, 143**

Journal article, Published version

Rad u časopisu, Objavljena verzija rada (izdavačev PDF)

Permanent link / Trajna poveznica: <https://um.nsk.hr/um:nbn:hr:237:423179>

Rights / Prava: [In copyright](#) / [Zaštićeno autorskim pravom.](#)

Download date / Datum preuzimanja: **2025-03-03**

Repository / Repozitorij:

[Repository of the Faculty of Civil Engineering,
University of Zagreb](#)



See discussions, stats, and author profiles for this publication at: <https://www.researchgate.net/publication/363366295>

Characterization of ground penetrating radar signal during simulated corrosion of concrete reinforcement

Article in *Automation in Construction* · November 2022

DOI: 10.1016/j.autcon.2022.104548

CITATIONS

19

READS

308

4 authors:



Ksenija Tesic

University of Zagreb Faculty of Civil Engineering

18 PUBLICATIONS 90 CITATIONS

[SEE PROFILE](#)



Ana Baricevic

University of Zagreb Faculty of Civil Engineering

69 PUBLICATIONS 702 CITATIONS

[SEE PROFILE](#)



Marijana Serdar

University of Zagreb

131 PUBLICATIONS 1,415 CITATIONS

[SEE PROFILE](#)

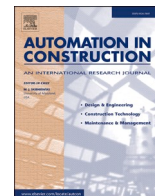


Nenad Gucunski

Rutgers, The State University of New Jersey

206 PUBLICATIONS 4,184 CITATIONS

[SEE PROFILE](#)



Characterization of ground penetrating radar signal during simulated corrosion of concrete reinforcement

Ksenija Tesic^a, Ana Baricevic^{a,*}, Marijana Serdar^a, Nenad Gucunski^b

^a University of Zagreb, Faculty of Civil Engineering, Department of Materials, Fra Andrije Kacica-Miosica 26, 10000 Zagreb, Croatia

^b Department of Civil and Environmental Engineering, Rutgers, The State University of New Jersey, 96 Frelinghuysen Road, Piscataway, NJ 08854, USA

ARTICLE INFO

Keywords:

Non-destructive testing
Ground penetrating radar
Corrosion
Concrete

ABSTRACT

In this paper, the adequacy of the experimental design in the accelerated corrosion process with the impressed current technique (IC) for ground penetrating radar (GPR) inspection was investigated. The aim of the study is to observe how the GPR signal amplitude behaves under different distributions of corrosion products generated by different exposure conditions in the IC technique. To investigate this, two different experimental setups were prepared. The results are summarized, discussed, and supported by visual evidence, other non-destructive techniques, and electromagnetic theory. The main finding is that the position of the sodium chloride solution required to ensure accelerated corrosion of the reinforcement determines the behaviour of the GPR signal, as it affects the position of the corrosion product layer and its distribution in the concrete cover.

1. Introduction

The designed and expected service life of reinforced concrete (RC) structures could be seriously compromised if adequate maintenance is not performed during their service. One of the main problems leading to disturbed service life of RC structures is corrosion of reinforcement [1–4]. Corrosion involves symbiotic processes in the concrete and on the surface of the reinforcement. In the case of chloride-induced corrosion, it starts with the penetration of chlorides into the concrete, which triggers the depassivation of the reinforcement once the chloride concentration reaches a critical level [5]. The inability to sustain the passive layer leads to a series of chemical reactions at the reinforcement, resulting in the formation of corrosion products, which in turn can cause cracking or even spalling of the concrete cover [6–8]. The optimal maintenance strategy should include the detection of corrosion during the initiation period to minimize the repair effort and the overall maintenance cost. However, complexity, duration of inspection, and ultimately costs, are often the main drivers for choosing a maintenance strategy. Infrastructure owners are often guided by cost alone and choose visual inspection as the only means of decision making, omitting that it is impossible to detect corrosion in the initial stages by visual inspection alone. Therefore, the use of appropriate non-destructive techniques (NDT) is a viable solution.

The attractiveness of non-destructive testing stems primarily from

the type of inspection and secondarily from the time required to perform it [9–11]. Nevertheless, in addition to the great accessibility, there should be a research community that ensures the reliability of the results and the continuous improvement of the techniques. One of the techniques that is constantly growing in the field of structural assessment is ground penetrating radar (GPR) [12–15]. The main role of GPR in civil engineering is to locate reinforcement and tendon ducts and to estimate the thickness of concrete cover. It is based on radiation of electromagnetic (EM) waves into the concrete and the detection of the echoes from an object or defect [16]. However, special efforts are made for corrosion characterization of reinforcement in RC structures using GPR [13,17–24]. The technique, which can simultaneously collect data on the location of reinforcement and corrosion condition, undoubtedly contribute to an effective maintenance strategy.

The principle of corrosion assessment with GPR is to observe the perturbation of reflected energy strength when comparing sound and corroded reinforcing bars. The reflected energy changes due to changes:

- i) at the interface between concrete and steel,
- ii) in the material.

The changes at the concrete-steel interface due to the corrosion of the rebars contribute to the changes in the reflection coefficient [25], so that the total reflection of the signal is different compared to sound rebars. In

* Corresponding author.

E-mail address: ana.baricevic@grad.unizg.hr (A. Baricevic).

addition, the changes in the condition of the surrounding concrete due to the causes and consequences of the corrosion process (e.g., water and chloride penetration, migration of corrosion products into the concrete cover, cracks, etc.) lead to changes in the registered amplitude of the echo. In particular, this leads to changes in the permittivity and conductivity of the concrete, which cause a change in the attenuation coefficient [26], further changing the strength of the echoes. The influence of water and chlorides in concrete on the strength of reflected energy has been proven by laboratory tests [27–32]. Furthermore, special efforts have been made to observe the effects of the formation of corrosion products around the rebars and their propagation in the concrete cover and to observe how they affect the change in the GPR signal [19,20,33–36]. Numerous studies have reported conflicting results on the effect of corrosion products on GPR signal amplitude, Table 1, and this has been discussed in detail in [18]. The corrosion process was usually accelerated in the laboratory using the impressed current technique (IC), Table 1, where the corrosion trigger is the applied potential difference between the observed rebar and another metal. Two main methods for acquiring the GPR attributes found in the literature are: a) monitoring during corrosion acceleration and b) data collection before and after corrosion acceleration. The experimental setup during corrosion acceleration also varied. In some of these studies, the rebars were exposed to current under dry conditions [20,34], while in most of these studies, the specimens were partially immersed in a sodium chloride solution below the rebar during the corrosion acceleration [19,20,36–38]. In the same studies, the GPR investigation was performed from the surface that was on the opposite side of the reinforcement from the solution level. It is in the nature of the impressed current technique that the experimental setup, e.g., the position of the electrodes and the solution level, affect the pattern of distribution of the corrosion products [39,40]. In the study [40] it was shown that the rust accumulation was more intense on the side facing the solution level. This means that the solution level below the reinforcement level produces a corrosion pattern that is different from natural corrosion [2]. Considering the principle of GPR, this could lead to misleading conclusions during GPR inspection if the current density and/or exposure time are not sufficient, especially when monitoring the corrosion process.

2. Research objective

Motivated by the above discussion, the main objective is formulated, Fig. 1. The main objective of this work is to investigate how different corrosion patterns due to different solution positions affect the GPR signal during an accelerated corrosion process with impressed current technique.

In the present study, two experimental setups were designed. The difference between the experimental setups was the position of the sodium chloride solution during the corrosion process. In the 1st experimental setup, the solution was below the reinforcement level as in most studies reported in the literature [19,20,36–38], while in the 2nd experimental setup it was above the reinforcement, considering the effect of solution on distribution of corrosion products [40]. In both experimental setups, parameters of the concrete that affect the GPR signal, such as the chloride content, moisture content, and crack width, were monitored while the corrosion parameters and the GPR signal were observed simultaneously.

3. Experimental program

3.1. Production of specimens

The specimens were prepared using cement CEM I 42.5 R, river aggregate (0/4 mm, 4/8 mm and 8/16 mm), potable water and chemical admixtures (superplasticizer and air-entraining admixture). The mix design and properties of fresh and hardened concrete are summarized in Table 2. Slump was determined after mixing, and compressive strength

Table 1

Review of laboratory studies on the influence of corrosion of reinforcement on GPR attributes, taken and adapted from [18].

Study	Technique for accelerated corrosion test	Method of acquiring the GPR attributes	Change in the GPR attributes	
			Trend of amplitude change	Main findings
Hubbard et al. [41]	Impressed current technique	Before and after corrosion acceleration	↓	Decrease in amplitude and increase in reflection travel time; the authors pointed out a possible influence of the wetting of the concrete cover during the experiment on the results.
Raju et al. [37]			↑	Increase in amplitude with a higher degree of corrosion and larger diameter of rebars. Established relationship between GPR amplitude and mass loss.
Zaki et al. [38]			↑↓	Different influence of corrosion process on GPR amplitude in rebars with different degrees of corrosion; the authors reported that the results could be influenced by the different moisture and chloride content in concrete.
Lai et al. [19]		Monitoring during corrosion acceleration	↑	Increase in amplitude and decrease in reflection travel time due to higher number of reflection points between concrete, steel, corrosion products, and cracks.
Zhan et al. [42]			↑	Increase in amplitude and decrease in reflection travel time. Established relationship between GPR amplitude and mass loss.
Hong et al. [20]			↑	Increase in amplitude and no change in peak frequency of the signal when corrosion products are formed.
Hong et al. [33]			↑	Increase in amplitude; more pronounced effect with increasing diameter of reinforcement. No effect of corrosion

(continued on next page)

Table 1 (continued)

Study	Technique for accelerated corrosion test	Method of acquiring the GPR attributes	Change in the GPR attributes	
			Trend of amplitude change	Main findings
Wong et al. [34]			↕	product formation on peak frequency. Increase in amplitude and then decrease as the crack widened.
Liu et al. [36]			↑	Increase in amplitude; the H-Alpha scattering classification was used to characterize the changes in signal with corrosion process. Decrease in amplitude and blurred hyperbola in the B-scan as a result of changes at the interface between concrete and steel.
Sossa et al. [35]	Corroded rebars cast in concrete	Before and after corrosion acceleration	↓	Decrease in amplitude and blurred hyperbola in the B-scan as a result of changes at the interface between concrete and steel and changes in the concrete due to rust, cracks and delamination.
	Curing chamber		↓	

after 28 days on 150 mm cube samples according to European standards [43,44].

The design of the specimens is shown in Fig. 2. The specimens were 700 mm × 300 mm × 250 mm, with two reinforcing bars ($\Phi/1 = 20 / 400$ mm) and a concrete cover of 50 mm. The sides of the specimens were coated with epoxy, as was the part of the rebar that was outside the specimens, Fig. 3a. The rebars had wires for electrical connection for the accelerated corrosion test, which were prepared before casting. The connection between the rebar and the wire was protected with an impermeable mastic, Fig. 3b.

3.2. Experimental setup for corrosion acceleration

The main objective of the experimental study was to characterize the changes in the GPR signal during accelerated corrosion of reinforcement in concrete using two different experimental designs. The main difference between the two experimental designs was the position of the aggressive sodium chloride solution during the accelerated corrosion process. The first experimental setup was selected as representative of the tests performed chosen to date replicate previously published research results [19,20,36–38], while the second experimental setup aimed to ensure distribution of the corrosion products in the concrete cover [40].

3.2.1. 1st experimental setup – chloride solution below corroding rebar

In the 1st experimental setup, specimens were first immersed in a container filled with 3.5% sodium chloride solution for 11 days. The immersion was intended to force the accumulation of chlorides on the surface, thus forcing the initiation of the corrosion process from above as soon as the rebar was exposed to the external current. After immersion,

the level of the solution was lowered below the level of the rebars. The specimens were left for 19 days to stabilize the moisture content throughout the concrete cover of the specimen. Then they were connected to an external power supply to accelerate the corrosion of the reinforcement. The total applied current was 0.038 A, which corresponds to a current density of 200 $\mu\text{A}/\text{cm}^2$. Three specimens were subjected to the accelerated corrosion process, which differed in the duration of the process. The duration was determined as a function of the targeted mass loss according to Faraday's law [45]. The targeted mass losses were 5%, 7.5% and 10%, corresponding to durations of the accelerated corrosion process of 39, 59 and 78 days, respectively.

3.2.2. 2nd experimental setup – chloride solution above corroding rebar

In the 2nd experimental setup, the 3.5% sodium chloride solution was placed in a container made of polystyrene sheets that occupied the entire top surface of the specimens. Initially, the solution was stored without a power supply for 5 days to stabilize the potential corresponding to the required current. By day 10, a total current of 0.114 A was applied, corresponding to a current density of 600 $\mu\text{A}/\text{cm}^2$. The higher current density, than in the 1st experimental setup, was intended to ensure a greater amount of corrosion products in the concrete cover. On the 10th day, the hairline crack appeared on the surface of the specimens. It was concluded that maintaining the higher current density (600 $\mu\text{A}/\text{cm}^2$) would probably lead to a sudden accumulation of corrosion products around the rebar without gradual migration into the concrete cover, which is not the case in reality. For this reason, the current was reduced to a value of 0.038 A, which corresponds to a current density of 200 $\mu\text{A}/\text{cm}^2$. In this experimental setup, three specimens were also subjected to the corrosion process for 39, 59, and 78 days. The arrangement of the 1st and 2nd experimental setups is shown in Table 3.

3.3. Assessment methods

The moisture and chloride content in the concrete cover were monitored along with the crack width during the corrosion acceleration process, as they have a great influence on all the corrosion attributes presented in this paper.

In the 1st experimental setup, relative humidity was monitored using the PosiTector CMM IS concrete moisture meter, with probes embedded at a depth of 50 mm. In the 2nd experimental setup, moisture content was determined by taking samples from the exposed surface. The samples were cylinders with a diameter of 18 mm and a height of 50 mm. The cylinders were cut to a height of 10 mm and then the mass of each piece was calculated (m_1), to obtain a gradual distribution of moisture in the concrete cover. The final moisture content w , where m_2 is the mass of each piece after drying to a constant weight, was determined as follows:

$$w = \frac{m_1 - m_2}{m_2} \cdot 100\% \quad (1)$$

Two different physical properties were measured in the two experimental setups. The sensors used to measure relative humidity in the 1st experimental setup were not applicable in the 2nd setup due to the submerged surface of the specimens. However, the relationship between these two properties is established [46,47].

The total chloride content was determined by potentiometric titration. First, the concrete powder was taken every 10 mm to a depth of 50 mm. A known amount of the concrete powder was placed in a beaker and mixed with 100 ml of deionized water and 10 ml of a 5 mol/l nitric acid (HNO_3) solution. The solution was then heated to boiling with constant stirring and stirred for another 3 min. The solution was then titrated with 0.1 M silver nitrate (AgNO_3).

Each moisture and chloride monitoring measurement was performed on one specimen from a series, assuming that the other specimens were exposed to the same conditions. During the corrosion process, the cylinders for moisture characterization were taken from the top of the

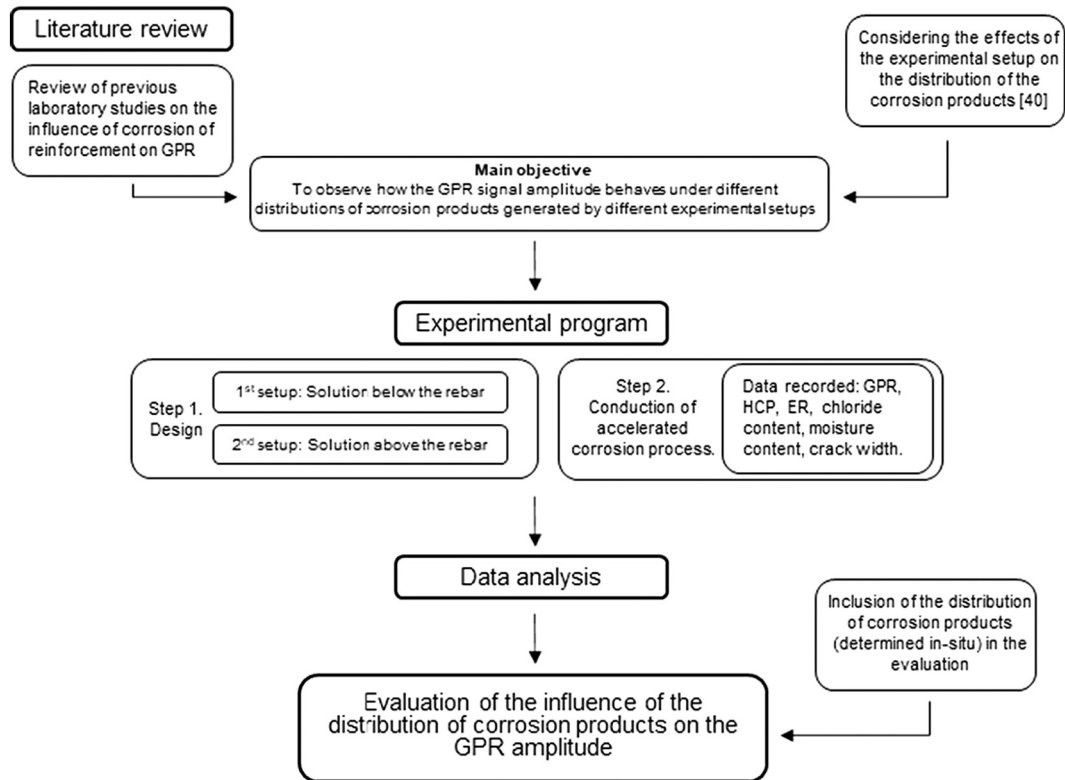


Fig. 1. Research methodology.

Table 2
Concrete mix design and properties of fresh and hardened concrete.

Concrete mix design						
Cement [kg/ m ³]	Potable water [kg/m ³]	River aggregate [kg/m ³]			Chemical admixtures [kg/m ³]	
		0/4 mm	4/8 mm	8/ 16 mm	superplasticizer	air- entraining admixture
401	121	843	501	579	2	1.6
Properties of fresh and hardened concrete						
Slump [mm]		Air-content [%]			Compressive strength with standard deviation [MPa]	
180		5			51.5 ± 3.4	

concrete near the edges of the specimen on the cathode rebar side. The concrete powder was taken near the anode. The sampling locations were chosen to be far enough to avoid the influence of the resulting holes on the GPR measurements.

Relative humidity and moisture content were determined on days 7, 10, 14, 28, 42, 56, and 70 of the corrosion process. Chloride content was determined on days 14, 28, 42, 56, and 70. In addition, chloride content was determined before the start of the accelerated corrosion process (day 0) for the 1st experimental setup and on days 7 and 10 for the 2nd experimental setup. Chlorides were also determined at the end of the corrosion process (days 39, 59, 78) for each specimen above the anode for both experimental setups.

Crack width was measured every 7 days, on day 10, and at the end of the testing period for each specimen using a crack width ruler at 5 points along the crack. The final value was determined as the average of 5 data points.

During the experiments, the current density and thus the applied current was kept constant, while the applied voltage varied according to the changes in the resistance of the specimens. For this reason, the change in voltage was also monitored. The data acquisition system was

set to record the voltage value every hour throughout the experiments.

3.3.1. Monitoring of corrosion attributes

GPR examination was performed every 7 days. In addition, it was performed on day 10 and at the end of the test period for each specimen. The GPR used in this study was Geophysical Survey Systems Inc. (GSSI) 2.7 GHz device. The scan interval of the instrument was 8 scans/cm, with the scan sampled in 512 data points. The scan range was 5 ns. The scans were processed using RADAN 7 software. The raw GPR data was processed with a bandpass filter and background removal. A constant one-point gain was also used.

In both experiments, data were collected from above. In the 2nd experimental setup, the solution was removed each time data were collected. The surface was cleaned with a cloth so that no excess water was visible on the surface. The GPR profiles were recorded perpendicular to the rebars. A total of 10 profiles were recorded each time, of which 5 were type A and 5 were type B (Fig. 4). Monitoring of reflected signal strength was based on observation of peak amplitudes derived from the scan over the anode rebar. The amplitudes were extracted and the final amplitude was determined as the average of 10 profiles. The amplitude is reported as normalized amplitude A in dB, expressed as

$$A = 20 \log_{10} \frac{A_t}{A_0} \quad [\text{dB}] \quad (2)$$

A_t – amplitude at time,

A_0 – amplitude before corrosion.

Monitoring of half-cell potential (HCP) as well as electrical resistivity (ER) was performed on the same days as GPR, except for the 2nd experimental setup before corrosion, where HCP and ER could not be measured due to extremely dry conditions. The half-cell potential is a semi-destructive technique for evaluating corrosion probability [48]. It is based on measuring of the potential difference between the reference electrode and the rebar. In this study, the Proceq Profometer Corrosion was used, and the reference electrode was the CSE (copper/copper

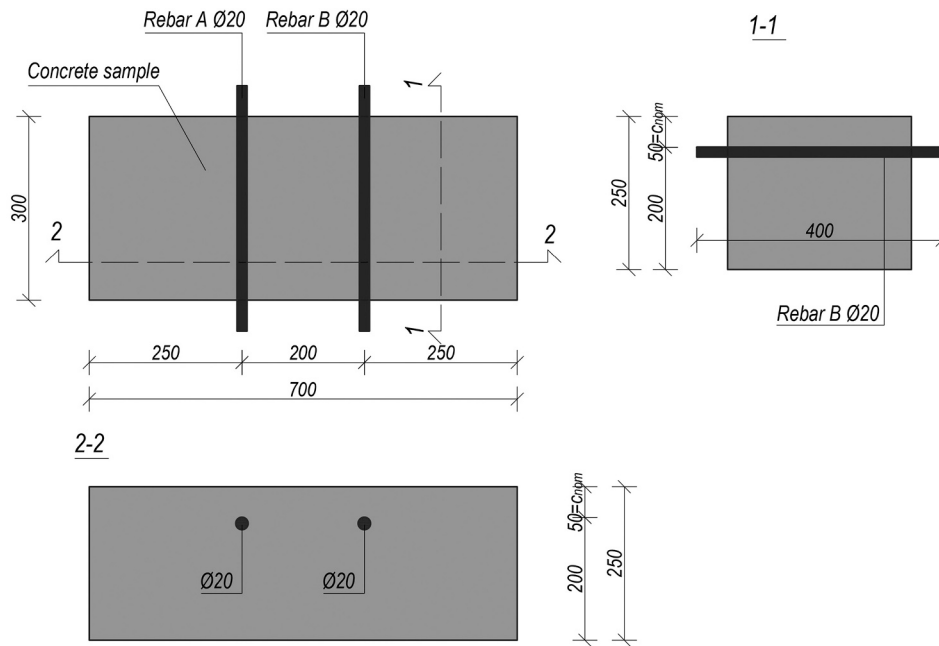


Fig. 2. Design of the specimen.

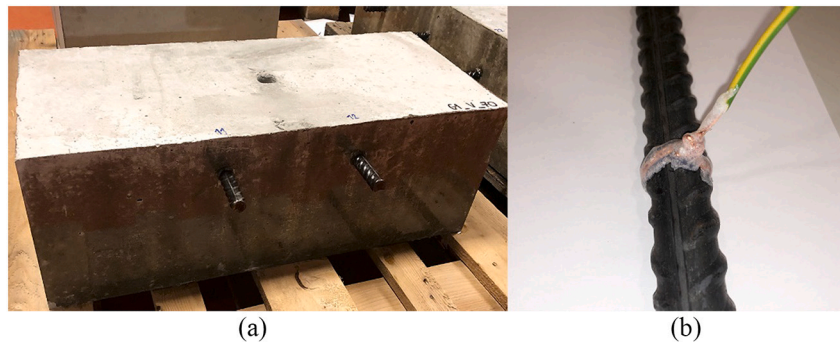


Fig. 3. a) Epoxy coated sides of the specimen, b) connection between rebar and wire.

sulphate electrode). During the measurement, the reference electrode was placed over the anode rebar. The potential values above -200 mV CSE indicate that the corrosion probability is $<10\%$, while it is $>90\%$ for values below -350 mV CSE [48].

Measuring the electrical resistivity of concrete is another method for assessing the corrosion risk [49]. Proceq Canin + Corrosion Analyzing Instrument with Wenner probe was used to measure the electrical resistivity of concrete. The resistivity was measured beyond the anode region with the probe oriented at a 45° to the direction of the rebar. If resistivity is $50\text{--}100$ $\text{k}\Omega\text{cm}$ the corrosion risk is low, $10\text{--}50$ $\text{k}\Omega\text{cm}$ - corrosion risk is moderate, and < 10 $\text{k}\Omega\text{cm}$ - corrosion risk is high [49].

In the 1st experimental setup, the surface was moistened 20 min before the measurements of HCP and ER. Both measurements were taken after GPR data collection was completed. During the GPR, HCP, and ER measurements, the anode and cathode were temporarily disconnected from the power supply.

4. Results

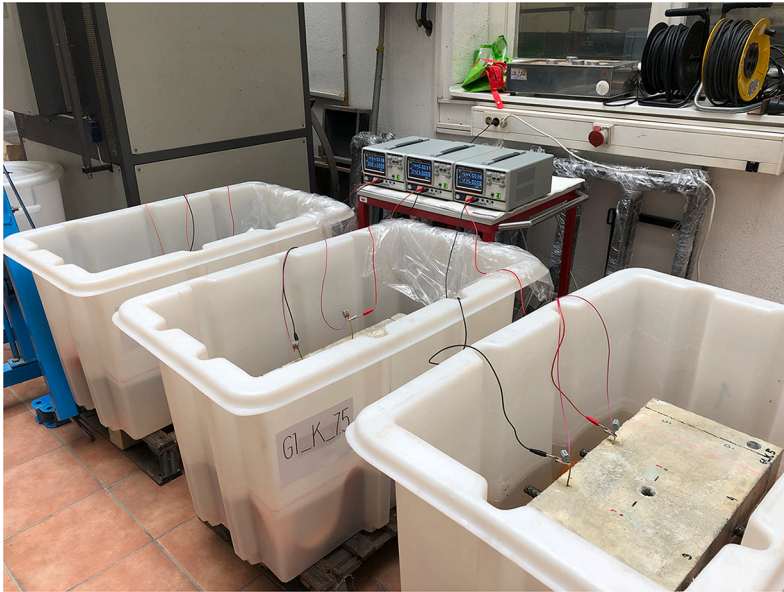
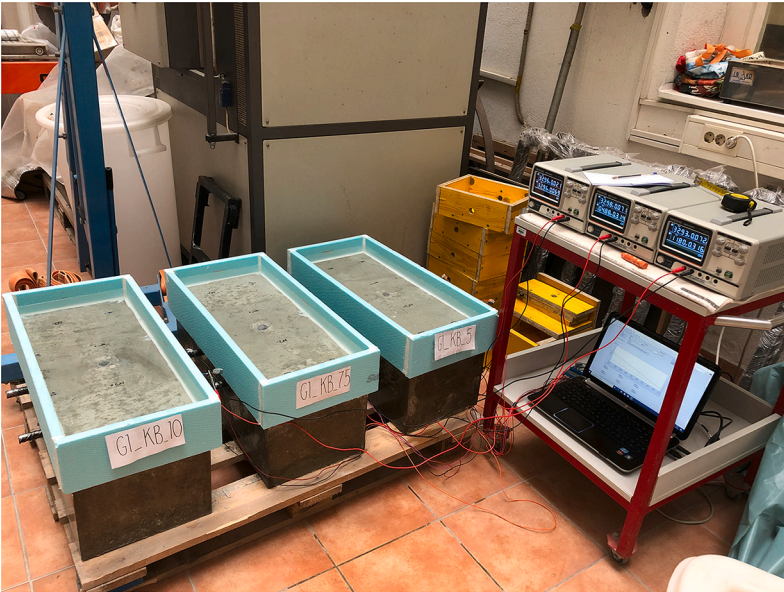
Relative humidity for 1st and moisture content for 2nd experimental setup during testing period are shown in Table 4.

In the 1st experimental setup, a high relative humidity of the concrete was maintained at the depth of the reinforcement, although the level of the sodium chloride solution was below the level of the

reinforcement. In the 2nd experimental setup, a stable moisture content in the concrete pores was observed only after seven days of the accelerated process and remained stable throughout the process. This is evident from the low value of the standard deviation around the average value of 4.8% for all depths. The distribution of moisture was such that there was no moisture gradient, but the moisture was evenly distributed over the concrete cover.

Fig. 5 shows the change in normalized amplitude (a), chloride content (b), crack width (c), resulting applied voltage (d), half-cell potential (e) and electrical resistivity (f) during the corrosion process for both setups. In general, the normalized GPR amplitude in the case of the 1st experimental setup did not show a significant change in value nor a clear trend of change during the evolution of the corrosion process. The changes were very subtle and ranged from -1.2 dB to 1.6 dB. From the chloride profiles, it can be concluded that the chloride content in the concrete cover showed the greatest change between days 0 and 14. While the specimens were immersed in the solution before the potential was applied, the chlorides accumulated in a shallow zone on the concrete surface. Once the potential was applied, it affected the migration of the chloride ions [2] so that the chloride content was uniformly distributed over all depths during the corrosion process. In addition, the chlorides from the solution that was under the rebars were able to migrate around the rebars. The formation of corrosion products, which have a larger volume than steel [50], leads to higher stresses around the

Table 3
Specimens subjected to the accelerated corrosion process in 1st and 2nd experimental setup.

	1st experimental setup	2nd experimental setup
		
Stabilization period without a power supply	11 days immersion in 3.5% sodium chloride solution	5 days exposure to 3.5% sodium chloride solution
Current density [$\mu\text{A}/\text{cm}^2$]	200	600, then 200 after 10 days
Duration [days]	39 59 78	39 59 78
Specimen	K1_5 K1_7.5 K1_10	K2_5 K2_7.5 K2_10

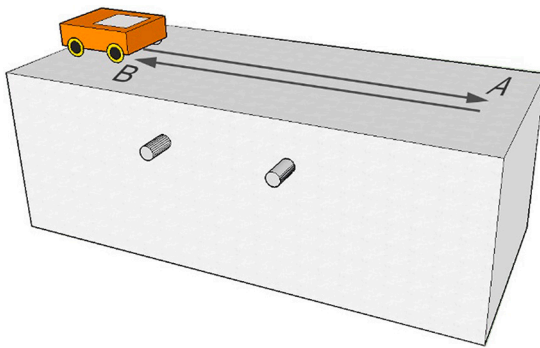


Fig. 4. GPR profiles orientation.

Table 4
Relative humidity and moisture content.

Day of accelerated corrosion process [days]	1st experimental setup Relative humidity RH [%]	2nd experimental setup Moisture content w [%]				
		0–10	10–20	20–30	30–40	40–50
		7	95.1	5.7	5.8	5.1
10	94.3	5.8	5.2	3.8	4.4	4.9
14	92	6.0	4.8	3.3	4.3	4.3
28	79.4	5.2	4.7	5.0	4.0	5.2
42	86.6	5.8	4.0	4.5	5.3	4.3
56	79.4	4.9	4.9	4.2	4.7	3.2
70	77.9	5.7	3.8	4.3	6.0	5.0
	RH mean value with standard deviation	w mean value with standard deviation				
	86.4 ± 7.5	4.8 ± 0.7				
	Corresponding w calculated from RH, according to [47]	Corresponding RH calculated from w, according to [47]				
	5.1	82.7				

rebars, which in turn leads to cracks in the concrete cover. The specimens were designed so that the crack was initiated from the top surface. Two out of three specimens from the 1st experimental setup showed longitudinal cracks above the anode bars. In addition, the specimens with cracks exhibited different behaviour, with the crack on K1_5 occurring 14 days before K1_7.5. Looking at the distribution of corrosion products shown in Table 5, it is clear that there was an initial disturbance in specimen K1_5. It appears that there was an initial defect at the interface between the reinforcement and the concrete that caused an accelerated accumulation of corrosion products on the left side of the specimen where the connection to the power supply was located. This caused the appearance of a wider crack on the top surface and was also noted by the faster decrease in the applied voltage for specimen K1_5 compared to specimen K1_7.5, while the current density remained constant (Fig. 5d). The applied voltage curves for the specimens with cracks were lower than the curve for the specimen without cracks, and this is more pronounced for the specimens where the crack occurred earlier. However, none of the effects described above had a significant effect on the GPR amplitude.

In contrast, different results were reported for the 2nd experimental setup. The GPR amplitudes for all three specimens followed a decreasing trend during the accelerated corrosion process. The largest decrease in amplitude was observed by day 10, where the curve showed a steep slope (see Fig. 5a). This is consistent with the higher current density applied by day 10 (Table 3). The decrease in amplitude continued after day 10, but at a slower rate. The specimen exposed to the accelerated corrosion process for the longest time exhibited the greatest signal loss, which was -11.5 dB on day 78 (corresponding to an amplitude loss of

73%). During the process, the chloride content in the concrete cover also changed, Fig. 5b. The chloride profiles taken near the anode showed a gradient in chloride content, while the profiles taken above the anode (at the end of each testing period; at 39, 59 & 78 day) at the end of the process showed a more uniform distribution. In addition, the chloride content values were higher above the anode. This is to be expected since there were cracks above the anode that allowed greater chloride penetration. In addition, the closer proximity of the anode affected the higher attraction of chloride ions. As for the development of cracks, the specimens of the 2nd experimental setup showed almost the same behaviour during the process. The cracks appeared on the 10th day and expanded at the same rate for all specimens. The resulting applied voltage (Fig. 5d) initially showed higher values corresponding to the higher current density (Table 3). The voltage corresponding to the specimen K2_5 was slightly lower than that of the other two specimens, Fig. 5d.

The value of the half-cell potential is an indicator of the ease of electron release [51], with more negative values indicating that the release is facilitated, suggesting a corrosion process. Considering the ASTM recommendation [48], the measured potential in both experiments was almost always below the of -350 mV value (Fig. 5e), indicating a corrosion process. The values for concrete resistivity show a similar behaviour (Fig. 5f). However, in this case, the different design of the experimental setups was reflected in slight differences in the resistivity values. The shift to a lower value for the 2nd experimental setup was most likely due to a higher chloride content [49], Fig. 5b, caused by the presence of sodium chloride solution at the top of the specimen. Nevertheless, the resistivity values were rather constant during the accelerated corrosion process and were around the value of 10 kΩcm.

5. Discussion

In this study, two different experimental setups were designed in which an accelerated corrosion process was carried out to monitor the effects of the process on the changes in GPR signal amplitude. In addition, several other methods were performed in parallel with GPR monitoring to substantiate the results. The results are discussed further with respect to two experimental setups.

For the 1st experimental setup, the GPR signal amplitude did not change significantly during the corrosion acceleration, while half-cell potential, electrical resistivity, and cracks occurrence result indicated an active corrosion process. At the end of the testing period, all specimens were opened at the location of the anode rebar to confirm corrosion activity. The specimen sections and the corrosion pattern through the anode are shown in Table 5. The corrosion pattern was considered for 2/3 of the bar in the centre of the specimen. On each side of the specimen, 5 cm is disregarded because the corrosion products present there are mainly the result of the pronounced corrosion at the contact between the rebar and the wires for electrical connection, as well as the leakage of the rebar on the outside of the contact with the concrete.

From the table above, it can be seen that the steel consumption due to corrosion, the formation of corrosion products and their migration in the 1st experimental setup occurred mainly below the rebar (84.5% for K1_5 and 94.3% for K1_7.5). Especially, when the orientation and position of GPR profiles is taken into account, Fig. 4. The position of the electrolyte in the 1st experimental arrangement forced the movement of chlorides from the electrolyte to the underside of the rebar and resulted in the reactions occurring mainly in this area. Furthermore, the location of corrosion reaction had an influence on the results obtained with the GPR. In fact, the propagation of the corrosion products from the bottom of the rebar affected the changes on the surface of the rebar and the surrounding concrete, which had a minor effect on the reflected GPR signal. This is because the metal, in this case the rebar, is considered a perfect reflector [52]. This means that when the electromagnetic waves encounter the reinforcement, they are completely reflected back to the receiving antenna. Thus, throughout the accelerated process, the scan above the anode represents the wave that has propagated only through

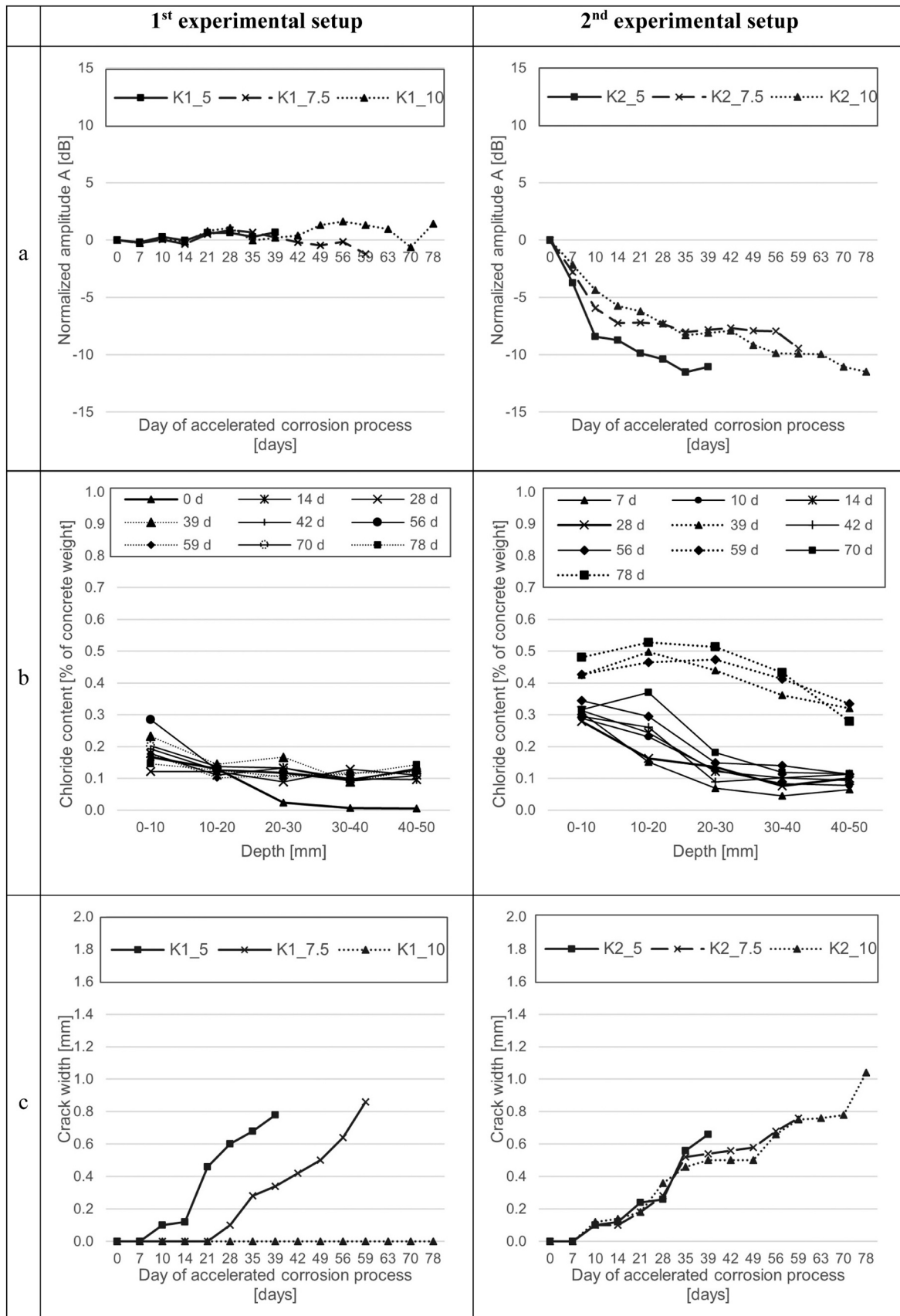


Fig. 5. a) Normalized GPR amplitude, b) chloride profiles, c) crack width, d) resulting applied voltage, e) half-cell potential and f) electrical resistivity during the corrosion process for samples designed according to the 1st experimental setup (diagrams on the left) and the 2nd experimental setup (diagrams on the right).

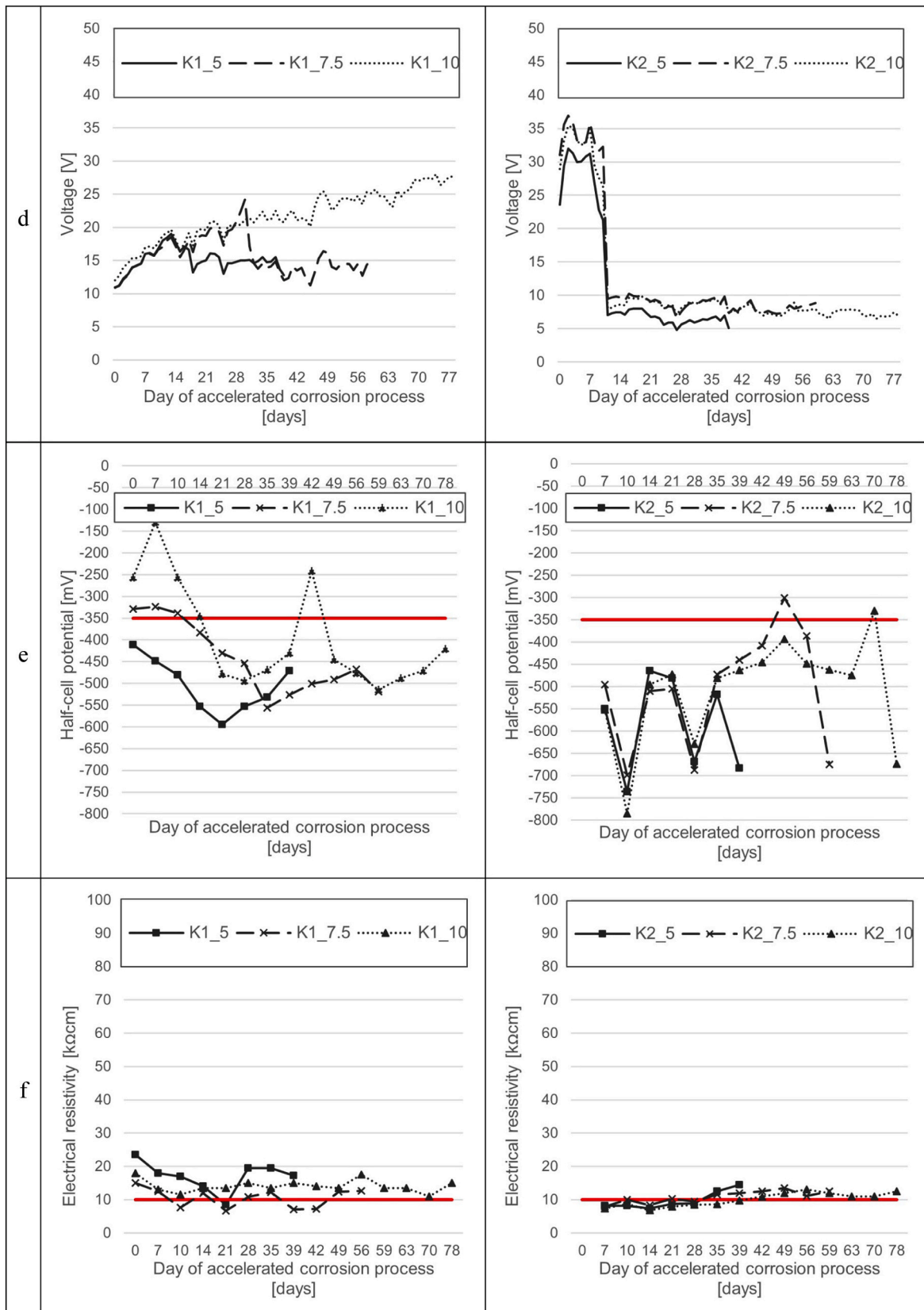
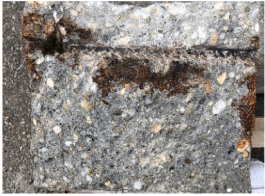












Fig. 5. (continued).

the concrete cover. In the case of the 1st experimental setup, the condition of the concrete cover was stable throughout the testing period, therefore the amplitude was also stable. First, the moisture content in

the concrete cover had stabilized after the drying period, which had no further effect on the change of amplitude. Second, and more importantly, the propagation of corrosion products from the bottom of the

Table 5
 Characterization of corrosion activity based on the sections through the anode bar.

Specimen	Section through the anode bar		Area under corrosion products	
	Figure of the cross section	Corrosion pattern in observed area	above the rebar	below the rebar
1st experimental setup				
K1_5			15.5%	84.5%
K1_7.5			5.7%	94.3%
K1_10		no corrosion detected		
2nd experimental setup				
K2_5			67.2%	32.8%
K2_7.5			73.8%	26.2%
K2_10			60%	40%

rebar could not affect the GPR signal since the signal did not reach this layer, because of the experimental arrangement with a perfect reflector, reinforcement, placed between the GPR and the corrosion layer.

In specimen K1_10, there was no significant corrosion of the reinforcement for reasons unknown to the authors, as shown in Table 5. The absence of cracks on the concrete surface proves this fact. This is an explanation for the slight amplitude divergence on day 35 between specimens K1_7.5 and K1_10. Comparing these two specimens, it is suspected that the widening of the cracks in specimen K1_7.5 after day 35 (Fig. 5c) began to affect the dispersion of the waves [34], resulting in a slight decrease in amplitude in this specimen. However, this deviation

is no longer observed in specimen K1_5 after the day 14, when a crack occurred. In summary, the results show that cracks up to 0.9 mm do not lead to a significant change in GPR response.

Considering the results and the discussion about this experimental setup, it can be concluded that this experimental arrangement cannot accurately represent corrosion-induced changes that would be relevant for monitoring with ground penetrating radar. Moreover, this corrosion case does not correspond to the actual corrosion state of reinforced concrete structures, where corrosion mainly occurs on the side of the rebar facing the concrete cover [2].

The results obtained with the GPR in the 2nd experimental

arrangement differed from those of the 1st experimental arrangement. Although the values of half-cell potential and concrete resistivity indicated that the corrosion process developed at the same rate as in the case of the 1st experimental setup, the gradual changes in the GPR signal were observed here. At the end of the testing period, all specimens were opened at the location of the anode rebar to confirm corrosion activity. The sections through the anode rebars are shown in [Table 5](#).

The first and the most important thing noted after opening the specimens was the distribution of the corrosion products. In this setup, the distribution of the corrosion products resembled more the natural corrosion of the reinforcement than the distribution in the first experiment, as the area under the corrosion products over the reinforcement was 67.2%, 73.8% and 60% for K2_5, K2_7.5 and K2_10, respectively. The products formed mainly at the top of the rebar and migrated through the concrete cover to the top of the specimen. The corrosion products had accumulated mostly in the narrow area around the rebar and gradually filled the pores of the concrete cover. The layer of corrosion products was most pronounced on the specimen with the highest degree of corrosion (K2_10).

The significant decrease in GPR amplitude strength that occurred in the 2nd experimental setup ([Fig. 5a](#)) was caused by several factors – water, chlorides dissolved in water, and corrosion products. This phenomenon can be explained by the reduction in amplitude due to: i) the change in the reflection coefficient of the steel and, ii) signal attenuation caused by changes in the properties of the surrounding concrete. The former is related to the change at the interface between concrete and steel, which is associated with the formation of corrosion products on the side of the reinforcement facing the concrete cover. Indeed, the amount of reflected energy at this surface is approximately equal to the contrast of the dielectric constants of these two materials [25]. The iron oxides have a lower dielectric constant than steel [52,53], so the energy reflected from the corrosion products in the narrow region of accumulation around the rebars is less than that of the noncorroding steel. As the signal propagates through the thin layer of accumulated corrosion products, it suffers additional signal loss as a result of additional propagation through the material [26]. Since the thickness of the corrosion product layer around the rebar is small, these reflections most likely overlap and result in an overall decrease in reflected energy.

The second cause of the significant reduction in amplitude is the combined action of water, chlorides dissolved in water, and corrosion products that have penetrated the concrete cover. These three affect the properties of the concrete in which the electromagnetic waves propagate. The electromagnetic properties of concrete, which is a mixture of different constituents, could be represented by the combined properties of solid particles, air, and water in the concrete pores [54]. After the specimen was treated with a sodium chloride solution from above, the ingress of the solution increased the amount of water in the concrete pores compared to the concrete before corrosion. It is known that this leads to a decrease in signal amplitude [30]. This effect is most pronounced in the first seven days and is associated with the amplitude decrease in [Fig. 5a](#). The moisture content stabilized after the seventh day ([Table 4](#)), so it can be assumed that changes in moisture content do not further affect the amplitude change. However, under the influence of the current applied to the rebars, the chlorides migrated from the solution into the concrete pores ([Fig. 5b](#)) and further increased the salinity of the water in the pores, resulting in additional attenuation due to the increased conductivity [26]. The migration of corrosion products into the pores of the concrete caused the air component in the mix being partially replaced by the corrosion product component, which further changed the dielectric properties of the mix. Comparing the dielectric properties of air and iron oxides, the iron oxides exhibit higher permittivity and conductivity [26,53,55], resulting in additional signal loss. Even though concrete is considered a non-magnetic material in most cases, the presence of iron oxides in materials such as magnetite can cause non-negligible attenuation [26]. These changes are most pronounced in the first 10 days and are related to the higher corrosion

rate of the reinforcement caused by the higher applied current density.

The last influencing factor is a crack, which appeared after the 10th day in all specimens above the anode. However, from the 1st experimental setup, it was concluded that a crack of up to 0.9 mm has a negligible effect on the dissipation of EM energy, so it is considered that it did not contribute significantly to the attenuation of the signal. The observed effect is in agreement with the numerical simulations on the influence of corrosion induced cracks on the GPR signal reported in [56]. There it was found that cracks up to 1 mm have a small effect on the GPR amplitude.

Based on the results obtained and the above discussion, it can be concluded that the solution facing the surface where the GPR inspection is performed is more suitable for observing the corrosion induced by the impressed current in the laboratory. The limitation of this study is the inevitable change in the salinity of the water in the concrete pores, which prevented the isolated effect of the spread of corrosion products on the GPR amplitude from being observed. Further studies will focus on isolating these two effects.

The ability of non-destructive methods to detect the corrosion process is highly dependent on the technique used. Half-cell potential and electrical resistivity detect corrosion regardless of the location of the corrosion layer with respect to the rebar and the concrete surface, while ground penetrating radar requires a change on the side of the rebar facing the concrete surface being tested. Therefore, in the second experimental setup, all non-destructive methods were able to detect the corrosion, while the GPR had sufficient resolution and stability in testing to detect the progression of the process over time, enabling quantitative analysis of the kinetics of the corrosion process over time.

Considering the real structures, the second experimental setup is closer to the natural evolution of the corrosion process, so the present study confirms that the GPR can be used to evaluate the corrosion of reinforcement in RC structures. However, certain limitations must be emphasised. It will be difficult to use the GPR as a stand-alone test method when evaluating structures for which historical data are not available and which are to be evaluated only once. In this case, the electrochemical methods, especially HCP, are more appropriate, even though they are destructive. If the testing of the structures extends over a longer period of time and is planned as a continuous monitoring of the structure, the GPR might be a better solution, as it provides a unique opportunity for non-destructive characterization of the corrosion kinetics. In addition, the GPR method could allow automation of the assessment of reinforced concrete structures. Currently, the limitations of GPR applications are the time-consuming data analysis and the insufficiently developed techniques for quantifying the reinforcement diameter.

6. Conclusion

In the present experimental study, the aim was to determine the influence of the different distributions of corrosion products caused by different experimental setups on the GPR signal amplitude in laboratory simulations. Due to the contradictory results on the influence of corrosion on the GPR signal reported in the literature, two experimental setups were designed: the first one replicates the setup of previous reported studies, and the second produces distribution closer to the natural corrosion process.

The results presented clearly show that the position of the sodium chloride solution during the accelerated corrosion process determines the location of corrosion products layer and their distribution in the concrete cover, which in turn determines the behaviour of the GPR signal. If the solution is below the rebar level, the formation of corrosion products occurs mainly from the bottom of the rebars. The migration of corrosion products also occurs mainly in the direction of the solution and deeper into the concrete. In that case, although all corrosion parameters clearly indicated corrosion propagation, the GPR amplitude did not change significantly. This can be attributed to the stable

condition of the concrete cover during the experiment and the inability of the signal to surpass fully reflective reinforcement to reach corrosion product layer. On the other hand, when the solution was at the top of the specimens, the formation of corrosion products and their migration is directed towards the upper surface of the concrete. In that case, the GPR amplitude had a decreasing trend throughout the corrosion propagation. The changes in GPR signal were influenced by the combined effect of changes at the interface between concrete and steel and changes in the material. Therefore, the second case better represents the corrosion of the reinforcement in real structures, as well as the changes that would be relevant for monitoring with ground penetrating radar. This experimental setup is more suitable for inspection with GPR in cases where corrosion is induced by impressed current technique. When comparing GPR with other electrochemical methods (HCP and ER), GPR was able to detect the progression of the corrosion process, while HCP and ER showed only minor changes in the progress of corrosion.

Further research is needed to isolate the effects of each material parameter (e.g. the moisture content, chlorides) independently to determine their contribution to the overall change in the GPR signal, and to observe the effects of the combined parameters to create different environmental conditions.

Funding

This research was funded by the European Union through the European Regional Development Fund's Competitiveness and Cohesion Operational Program, grant number KK.01.1.1.04.0041, project "Autonomous System for Assessment and Prediction of infrastructure integrity (ASAP)".

Declaration of Competing Interest

The authors declare that they have no known competing financial interests or personal relationships that could have appeared to influence the work reported in this paper.

Data availability

Data will be made available on request.

References

- [1] M. Alexander, H. Beushausen, Durability, service life prediction, and modelling for reinforced concrete structures – review and critique, *Cem. Concr. Res.* 122 (2019) 17–29, <https://doi.org/10.1016/j.cemconres.2019.04.018>.
- [2] L. Bertolini, B. Elsener, P. Pedeferrì, R.B. Polder, *Corrosion of Steel in Concrete: Prevention, Diagnosis, Repair*, Wiley, Weinheim, 2003. ISBN: 9783527308002.
- [3] X. Shi, N. Xie, K. Fortune, J. Gong, Durability of steel reinforced concrete in chloride environments: an overview, *Constr. Build. Mater.* 30 (2012) 125–138, <https://doi.org/10.1016/j.conbuildmat.2011.12.038>.
- [4] D. Banic, D. Bjegovic, G. Balabanic, Study of corrosion rate in reinforced-concrete, *Gradevinar J. Croat. Assoc. Civ. Eng.* 60 (2008) 123–132.
- [5] U. Angst, B. Elsener, C.K. Larsen, Ø. Vennesland, Critical chloride content in reinforced concrete - a review, *Cem. Concr. Res.* 39 (2009) 1122–1138, <https://doi.org/10.1016/j.cemconres.2009.08.006>.
- [6] S. Ahmad, Reinforcement corrosion in concrete structures, its monitoring and service life prediction - a review, *Cem. Concr. Compos.* 25 (2003) 459–471, [https://doi.org/10.1016/S0958-9465\(02\)00086-0](https://doi.org/10.1016/S0958-9465(02)00086-0).
- [7] M. Otieno, H. Beushausen, M. Alexander, Chloride-induced corrosion of steel in cracked concrete – part I: experimental studies under accelerated and natural marine environments, *Cem. Concr. Res.* 79 (2016) 373–385, <https://doi.org/10.1016/j.cemconres.2015.08.009>.
- [8] D. Bjegovic, M. Serdar, A. Baricevic, M.J. Rukavina, Assessing condition of concrete pier after three decades of exposure to sea water, *Gradevinar J. Croat. Assoc. Civ. Eng.* 67 (2015) 1155–1164, <https://doi.org/10.14256/JCE.1188.2014>.
- [9] M. Solla, B. Riveiro, P. Arias, H. Lorenzo, Introduction, in: B. Riveiro, M. Solla (Eds.), *Non-Destructive Techniques for the Evaluation of Structures and Infrastructure*, first ed., CRC Press, London, 2016, pp. 3–6, <https://doi.org/10.1201/b19024>.
- [10] D.M. McCann, M.C. Forde, Review of NDT methods in the assessment of concrete and masonry structures, *NDT & E Int.* 34 (2001) 71–84, [https://doi.org/10.1016/S0963-8695\(00\)00032-3](https://doi.org/10.1016/S0963-8695(00)00032-3).
- [11] S. Abu Dabous, S. Feroz, Condition monitoring of bridges with non-contact testing technologies, *Autom. Constr.* 116 (2020), 103224, <https://doi.org/10.1016/j.autcon.2020.103224>.
- [12] T. Omar, M.L. Nehdi, T. Zayed, Performance of NDT techniques in appraising condition of reinforced concrete bridge decks, *J. Perform. Constr. Facil.* 31 (2017) 04017104, [https://doi.org/10.1061/\(asce\)cf.1943-5509.0001098](https://doi.org/10.1061/(asce)cf.1943-5509.0001098).
- [13] A. Tarussov, M. Vandry, A. De La Haza, Condition assessment of concrete structures using a new analysis method: ground-penetrating radar computer-assisted visual interpretation, *Constr. Build. Mater.* 38 (2013) 1246–1254, <https://doi.org/10.1016/j.conbuildmat.2012.05.026>.
- [14] K. Dinh, N. Gucunski, T.H. Duong, An algorithm for automatic localization and detection of rebars from GPR data of concrete bridge decks, *Autom. Constr.* 89 (2018) 292–298, <https://doi.org/10.1016/j.autcon.2018.02.017>.
- [15] W.W.-L. Lai, X. Dérobert, P. Annan, A review of ground penetrating radar application in civil engineering: a 30-year journey from locating and testing to imaging and diagnosis, *NDT & E Int.* 96 (2018) 58–78, <https://doi.org/10.1016/j.ndteint.2017.04.002>.
- [16] D.J. Daniels, *Ground Penetrating Radar, second ed.*, The Institution of Electrical Engineers, London, 2004. ISBN: 9780863413605.
- [17] K. Dinh, N. Gucunski, J. Kim, T.H. Duong, Understanding depth-amplitude effects in assessment of GPR data from concrete bridge decks, *NDT & E Int.* 83 (2016) 48–58, <https://doi.org/10.1016/j.ndteint.2016.06.004>.
- [18] K. Tesic, A. Baricevic, M. Serdar, Non-destructive corrosion inspection of reinforced concrete using ground-penetrating radar: a review, *Materials (Basel)*. 14 (2021) 975, <https://doi.org/10.3390/ma14040975>.
- [19] W.-L. Lai, T. Kind, M. Stoppel, H. Wiggenhauser, Measurement of accelerated steel corrosion in concrete using ground-penetrating radar and a modified half-cell potential method, *J. Infrastruct. Syst.* 19 (2013) 205–220, [https://doi.org/10.1061/\(ASCE\)IS.1943-555X.0000083](https://doi.org/10.1061/(ASCE)IS.1943-555X.0000083).
- [20] S. Hong, W.W.-L. Lai, G. Wilsch, R. Helmerich, R. Helmerich, T. Günther, H. Wiggenhauser, Periodic mapping of reinforcement corrosion in intrusive chloride contaminated concrete with GPR, *Constr. Build. Mater.* 66 (2014) 671–684, <https://doi.org/10.1016/j.conbuildmat.2014.06.019>.
- [21] C.L. Barnes, J.F. Trottier, D. Forgeron, Improved concrete bridge deck evaluation using GPR by accounting for signal depth-amplitude effects, *NDT & E Int.* 41 (2008) 427–433, <https://doi.org/10.1016/j.ndteint.2008.03.005>.
- [22] N. Gucunski, F. Romero, S. Kruschwitz, R. Feldmann, A. Abu-Hawash, M. Dunn, Multiple complementary nondestructive evaluation Technologies for Condition Assessment of concrete bridge decks, *Transp. Res. Rec.* (2010) 34–44, <https://doi.org/10.3141/2201-05>.
- [23] K. Dinh, N. Gucunski, J. Kim, T.H. Duong, Method for attenuation assessment of GPR data from concrete bridge decks, *NDT & E Int.* 92 (2017) 50–58, <https://doi.org/10.1016/j.ndteint.2017.07.016>.
- [24] K. Dinh, N. Gucunski, Factors affecting the detectability of concrete delamination in GPR images, *Constr. Build. Mater.* 274 (2021), 121837, <https://doi.org/10.1016/j.conbuildmat.2020.121837>.
- [25] ACI Committee 228, *Nondestructive Test Methods for Evaluation of Concrete in Structures*, American Concrete Institute, Farmington Hills, MI, 1998. <https://www.concrete.org/publications/internationalconcreteabstractsportal/m/detail/s/id/5119>. (Accessed 10 July 2021).
- [26] N.J. Cassidy, Electrical and magnetic properties of rocks, soils and fluids, in: H. M. Jol (Ed.), *Ground Penetrating Radar Theory and Applications*, Elsevier, Amsterdam, 2009, pp. 41–72, <https://doi.org/10.1016/B978-0-444-53348-7.00002-8>.
- [27] S. Laurens, J.P. Balayssac, J. Rhazi, G. Klysz, G. Arliguie, Non-destructive evaluation of concrete moisture by GPR: experimental study and direct modeling, *Mater. Struct.* 38 (2005) 827–832, <https://doi.org/10.1007/BF02481655>.
- [28] G. Klysz, J.P. Balayssac, Determination of volumetric water content of concrete using ground-penetrating radar, *Cem. Concr. Res.* 37 (2007) 1164–1171, <https://doi.org/10.1016/j.cemconres.2007.04.010>.
- [29] X. Dérobert, J. Jaquinta, G. Klysz, J.P. Balayssac, Use of capacitive and GPR techniques for the non-destructive evaluation of cover concrete, *NDT & E Int.* 41 (2008) 44–52, <https://doi.org/10.1016/j.ndteint.2007.06.004>.
- [30] S.F. Senin, R. Hamid, Ground penetrating radar wave attenuation models for estimation of moisture and chloride content in concrete slab, *Constr. Build. Mater.* 106 (2016) 659–669, <https://doi.org/10.1016/j.conbuildmat.2015.12.156>.
- [31] J. Hugenschmidt, R. Loser, Detection of chlorides and moisture in concrete structures with ground penetrating radar, *Mater. Struct.* 41 (2008) 785–792, <https://doi.org/10.1617/s11527-007-9282-5>.
- [32] S. Laurens, J.P. Balayssac, J. Rhazi, G. Arliguie, Influence of concrete relative humidity on the amplitude of ground-penetrating radar (GPR) signal, *Mater. Struct.* 35 (2002) 198–203, <https://doi.org/10.1007/BF02533080>.
- [33] S. Hong, W.-L. Lai, R. Helmerich, Experimental monitoring of chloride-induced reinforcement corrosion and chloride contamination in concrete with ground-penetrating radar, *Struct. Infrastruct. Eng.* 11 (2015) 15–26, <https://doi.org/10.1080/15732479.2013.879321>.
- [34] P.T.W. Wong, W.W.L. Lai, J.F.C. Sham, C. Poon, Hybrid non-destructive evaluation methods for characterizing chloride-induced corrosion in concrete, *NDT & E Int.* 107 (2019), 102123, <https://doi.org/10.1016/j.ndteint.2019.05.008>.
- [35] V. Sossa, V. Pérez-Gracia, R. González-Drigo, M.A. Rasol, Lab non destructive test to analyze the effect of corrosion on ground penetrating radar scans, *Remote Sens.* 11 (2019) 2814, <https://doi.org/10.3390/rs11232814>.
- [36] H. Liu, J. Zhong, F. Ding, X. Meng, C. Liu, J. Cui, Detection of early-stage rebar corrosion using a polarimetric ground penetrating radar system, *Constr. Build. Mater.* 317 (2022), 125768, <https://doi.org/10.1016/j.conbuildmat.2021.125768>.

- [37] R.K. Raju, M.I. Hasan, N. Yazdani, Quantitative relationship involving reinforcing bar corrosion and ground-penetrating radar amplitude, *ACI Mater. J.* 115 (2018) 449–457, <https://doi.org/10.14359/51702187>.
- [38] A. Zaki, M.A.M. Johari, W.M.A.W. Hussin, Y. Jusman, Experimental assessment of rebar corrosion in concrete slab using ground penetrating radar (GPR), *Int. J. Corros.* 2018 (2018) 5389829, <https://doi.org/10.1155/2018/5389829>.
- [39] C. Fu, N. Jin, H. Ye, J. Liu, X. Jin, Non-uniform corrosion of steel in mortar induced by impressed current method: an experimental and numerical investigation, *Constr. Build. Mater.* 183 (2018) 429–438, <https://doi.org/10.1016/j.conbuildmat.2018.06.183>.
- [40] J. Chen, C. Fu, H. Ye, X. Jin, Corrosion of steel embedded in mortar and concrete under different electrolytic accelerated corrosion methods, *Constr. Build. Mater.* 241 (2020), 117971, <https://doi.org/10.1016/j.conbuildmat.2019.117971>.
- [41] S.S. Hubbard, J. Zhang, P.J.M. Monteiro, J.E. Peterson, Y. Rubin, Experimental detection of reinforcing Bar corrosion using nondestructive geophysical techniques, *ACI Mater. J.* 100 (2003) 501–510, <https://doi.org/10.14359/12957>.
- [42] B.J. Zhan, W.W.L. Lai, S.C. Kou, C.S. Poon, W.F. Tsang, Correlation between accelerated steel corrosion in concrete and ground penetrating radar parameters, in: C. Leung, K.T. Wan (Eds.), *International RILEM Conference on Advances in Construction Materials through Science and Engineering*, RILEM Publications SARL, Hong Kong, China, 2011.
- [43] HZN Standards Publications, HRN EN 12350–2:2019, Testing fresh concrete – Part 2: Slump-test, Croatian Standards Institute, Zagreb, 2019. <https://repositorij.hzn.hr/norm/HRN+EN+12350-2%3A2019> (accessed October 8, 2021).
- [44] HZN Standards Publications, HRN EN 12390–3:2019, Testing Hardened Concrete - Part 3: Compressive Strength of Test Specimens, Croatian Standards Institute, Zagreb, 2019. <https://repositorij.hzn.hr/norm/HRN+EN+12390-3%3A2019> (accessed October 8, 2021).
- [45] T.A. El Maaddawy, K.A. Soudki, Effectiveness of impressed current technique to simulate corrosion of steel reinforcement in concrete, *J. Mater. Civ. Eng.* 15 (2003) 41–47, [https://doi.org/10.1061/\(ASCE\)0899-1561\(2003\)15:1\(41\)](https://doi.org/10.1061/(ASCE)0899-1561(2003)15:1(41)).
- [46] C. Andrade, J. Sarria, C. Alonso, Relative humidity in the interior of concrete exposed to natural and artificial weathering, *Cem. Concr. Res.* 29 (1999) 1249–1259, [https://doi.org/10.1016/S0008-8846\(99\)00123-4](https://doi.org/10.1016/S0008-8846(99)00123-4).
- [47] M. Cunningham, When is a concrete slab dry enough?, in: *Build*, April/May, 2008, pp. 25–26, B105–25-DrySlab.pdf, buildmagazine.org.nz. (Accessed 8 October 2021).
- [48] ASTM, C876–91: Standard Test Method for Half-Cell Potentials of Uncoated Reinforcing Steel in Concrete. <https://www.astm.org/c0876-91r99.html>, 1999. (Accessed 8 October 2021).
- [49] R. Polder, C. Andrade, B. Elsener, Ø. Vennesland, J. Gulikers, R. Weidert, M. Raupach, Test methods for on site measurement of resistivity of concrete, *Mater. Struct.* 33 (2000) 603–611, <https://doi.org/10.1007/BF02480599>.
- [50] A. Poursaei, Corrosion of steel in concrete structures, in: A. Poursaei (Ed.), *Corrosion of Steel in Concrete Structures*, Elsevier, London, 2016, pp. 19–33, <https://doi.org/10.1016/B978-1-78242-381-2.00002-X>.
- [51] A. Poursaei, C.M. Hansson, Potential pitfalls in assessing chloride-induced corrosion of steel in concrete, *Cem. Concr. Res.* 39 (2009) 391–400, <https://doi.org/10.1016/j.cemconres.2009.01.015>.
- [52] D.J. Clem, T. Schumacher, J.P. Deshon, A consistent approach for processing and interpretation of data from concrete bridge members collected with a hand-held GPR device, *Constr. Build. Mater.* 86 (2015) 140–148, <https://doi.org/10.1016/j.conbuildmat.2015.03.105>.
- [53] W.M. Haynes, *CRC Handbook of Chemistry and Physics*, 97th ed., CRC Press, Boca Raton, 2017. ISBN: 9781498754286.
- [54] U.B. Halabe, K. Maser, E.A. Kausel, Propagation characteristics of electromagnetic waves in concrete, in: *Massachusetts Institute of Technology, Civil Engineering, Report No.: ARO 2462U.3-EG-UIR*, 1989.
- [55] R.M. Cornell, U. Schwertmann, *The Iron Oxides*, Wiley, Weinheim, 2003. ISBN: 9783527302741.
- [56] S. Hong, D. Chen, B. Dong, Numerical simulation and mechanism analysis of GPR-based reinforcement corrosion detection, *Constr. Build. Mater.* 317 (2022), 125913, <https://doi.org/10.1016/j.conbuildmat.2021.125913>.